Structurally coupled inversion of ERT and refraction seismic data combined with cluster-based model integration

Hellman, Kristofer; Ronczka, Mathias; Günther, Thomas; Wennermark, Marcus; Rücker, Carsten; Dahlin, Torleif

Published in:
Journal of Applied Geophysics

DOI:
10.1016/j.jappgeo.2017.06.008

2017

Document Version:
Publisher's PDF, also known as Version of record

Journal of Applied Geophysics 143 (2017) 169–181

Contents lists available at ScienceDirect

Journal of Applied Geophysics

journal homepage: www.elsevier.com/locate/jappgeo

Structurally coupled inversion of ERT and refraction seismic data combined with cluster-based model integration

Kristofer Hellman[a,*], Mathias Ronczka[a], Thomas Günther[b], Marcus Wennermark[a], Carsten Rücker[c], Torleif Dahlin[a]

[a] Engineering Geology, Lund University, Box 118, Lund SE-221 00, Sweden
[b] Leibniz Institute for Applied Geophysics, Stilleweg 2, Hannover D-30655, Germany
[c] Technische Universität Berlin, Ernst-Reuter-Platz 1, D-10587 Berlin, Germany

ARTICLE INFO

Article history:
Received 15 November 2016
Received in revised form 30 May 2017
Accepted 16 June 2017
Available online 19 June 2017

Keywords:
ERT
Refraction seismics
Structurally coupled inversion
Joint inversion
Cluster analysis

ABSTRACT

Electrical resistivity tomography (ERT) and refraction seismics are among the most frequently used geophysical methods for site-investigations and the combined results can be very helpful to fill in the gaps between the point measurements made by traditional geotechnical methods such as Cone Penetration Test (CPT), core-drilling and geophysical borehole logging. The interpretation of the results from a geophysical investigation constituting a single method often yields ambiguous results. Hence, an approach utilizing multiple techniques is often necessary. To facilitate interpretation of such a combined dataset, we propose a more controlled and objective approach and present a method for a structurally coupled inversion of 2D electrical resistivity and refraction seismic data using unstructured meshes. Mean shift clustering is used to combine the two images and to compare the separate and coupled inversion methodologies. Two synthetic examples are used to demonstrate the method, and a field-data example is included as a proof of concept. In all cases a significant improvement by the coupling is visible. The methodology can be used as a tool for improved data interpretation and for obtaining a more comprehensive and complete picture of the subsurface by combining geophysical methods.

1. Introduction

Geophysical methods have proved valuable for the site investigations in large projects (e.g., Dahlin et al., 1999; Cavinato et al., 2006; Danielsen, 2010; Di and Wang, 2010). Especially the combined usage of Electrical Resistivity Tomography (ERT) and refraction seismics is a feasible methodology for site investigations in preparation for tunneling and road-building in Scandinavia (Dahlin et al., 1999). The underlying motivation for combining two methods based on different physical properties is the possibility to decrease the inherent ambiguities of each method (Linder et al., 2010). Ambiguities with ERT could be, for example, failure to detect a low-contrast resistivity boundary between a layer of shale and a layer of clay. In this case, seismic profiling could possibly detect this boundary due to a high contrast in seismic velocity. The joint inversion of two separate datasets may also assist in improving the overall resolution, creating models that are in better agreement with each other, thus assisting the interpretation (e.g., Gallardo and Meju, 2004).

The use of more than one geophysical dataset for geophysical inversion was first presented by Vozoff and Jupp (1975). This should ideally result in a single subsurface model that can explain the used datasets (Lines et al., 1988). Several methods to perform joint or cooperative inversions have been developed (e.g., Lines et al., 1988, Haber and Oldenburg, 1997, Bosch, 1999, Paasche and Tronicke, 2007, Gallardo and Meju, 2011). Utilizing data from several geophysical methods can be done in three main ways: i) joint interpretation using different datasets that are separately inverted, ii) joint inversion of separate data sets for a common parameter, iii) coupled inversion, where separate datasets constrain each other (Doetsch et al., 2012) .The joint interpretation approach suffers from ambiguities inherent in the model parameters. However, statistical tools could provide a more objective method to analyse the data (e.g., Tronicke et al., 2004, Paasche et al., 2006, Bedrosian et al., 2007). This approach is applied here in the post-processing stage as described in the methodology of this paper. The question after the kind of results is also a very important part of formulating the inverse problem. There is a possibility not only to look for major geophysical structures in the data and hence create high resolution models which can aid

* Corresponding author.
E-mail address: kristofer.hellman@tg.lth.se (K. Hellman).

http://dx.doi.org/10.1016/j.jappgeo.2017.06.008
0926-9851/

the interpreter in finding for example a ground water surface. The additional use of petrophysical links between a geophysical property such as a certain resistivity, empirically linked to a specific hydraulic property through Archie's law could also be a possible outcome.

The underlying hypothesis for the combination of electrical and seismic data, is a correlation between resistivity and velocity. Archie (1942) and Wyllie et al. (1956) investigated the relationship between geophysical parameters and the porosity and thus confirmed indirectly the main assumption for a joint inversion of seismic and ERT. This is due to the influence on both of these geophysical parameters from the pore structure of the materials (e.g., Meju et al., 2003).

Our methodology represents a mutually and structurally coupled cooperative inversion approach. This means that the structural pattern in one model is used to guide the inversion of the other and vice versa. Structural coupled inversion goes back to Zhang and Morgan (1996) and Haber and Oldenburg (1997). They minimize, additionally to the individual objective functions, a measure of dissimilarity of the models. Another popular joint inversion method is called cross-gradients (Gallardo and Meju, 2004), where model gradients in two images are penalized only if they go into different directions. The cross-gradient method was originally designed for regular grids, but was later extended to irregular meshes (Lelivre et al., 2012). Here we follow yet another idea originally introduced by Günther and Rücker (2006) that does not need an additional objective function, but works through adaption of smoothness matrices. A similar approach with ERT and surface wave seismic data was demonstrated by Wisén and Christiansen (2005).

The presented joint inversion algorithm leads to two or more model sections, which are used for a cluster analysis for further interpretation. The clustering is utilized to create a unified, automatic, numerical interpretation of the surveyed profile. Using clustering algorithms to aid interpretation has been shown to be a step towards a more automated and less ambiguous interpretation (e.g., Tronicke et al., 2004, Paasche and Tronicke, 2007, Linder et al., 2010).

This article elaborates on the rather coarse ideas presented in Günther and Rücker (2006) and Günther et al. (2010), further extending them to a complete interpretive framework that is able to work on irregular triangular meshes. There are two main benefits of using these meshes: 1) a more computationally efficient cell division with local refinement, and 2) the possibility to include, without further adaptations, surface topography or known subsurface geometry.

In order to provide a basis for the validation of the method presented here, two separate synthetic geophysical scenarios have been created. All the modeling, data analysis and inversions within the scope of this article were carried out with the help of software that is freely available to the scientific community (Rücker and Günther, 2010-2016). Finally, a field case is presented demonstrating the ability of the approach to deal with real data.

2. Methodology

The methodology consists of three major parts: 1) Numerical modeling to generate synthetic resistivity and refraction seismic data for different models, 2) the inverse modeling scheme, for separate and structurally coupled inversion of resistivity and refraction seismic data, and 3) mean shift cluster analysis for a final presentation of major units.

2.1. Synthetic resistivity forward modeling

The governing partial differential equation relating the potential u as a result of current injection $\mathbf{j}$ and the conductivity σ reads:

$$\Delta\cdot(\sigma\nabla u) = -\nabla\cdot\mathbf{j} \text{ in } \Omega \subset \mathbb{R}^3 \quad (1)$$

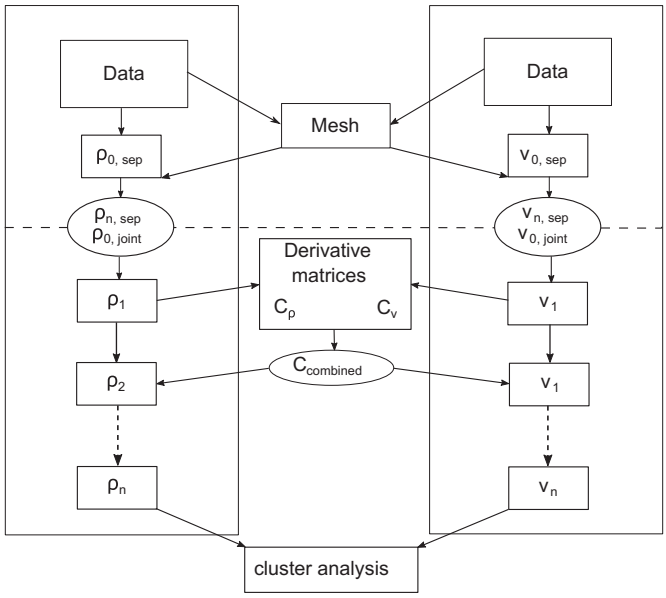

Fig. 1. Schematic view of structurally coupled inversion approach leading to cluster analysis.

Even though the resistivity distribution is two-dimensional, i.e., constant along y, the point source is inherently three-dimensional. Therefore the potential u is transformed into wave-number domain and solved for a series of wave numbers k_y.

$$\Delta\cdot(\sigma\nabla u) - k_y^2\sigma u = -1/2\nabla\cdot\mathbf{j} \text{ in } \Omega \subset \mathbb{R}^3 \quad (2)$$

We follow the suggestion of Kemna (2000) combining Gaussian quadrature and Laguerre point integration. The individual wavenumber equations are solved by Finite Elements on triangular meshes.

We make use of the secondary potential (SP) approach (Rücker et al., 2006), i.e. only the deviation from a homogeneous half-space is computed which allows much coarser meshes for inversion. According to Günther et al. (2006), once at the beginning of the inversion, the potentials for a conductivity $\sigma = 1$ S/m are computed on a highly refined mesh. In the course of inversion, SP calculation

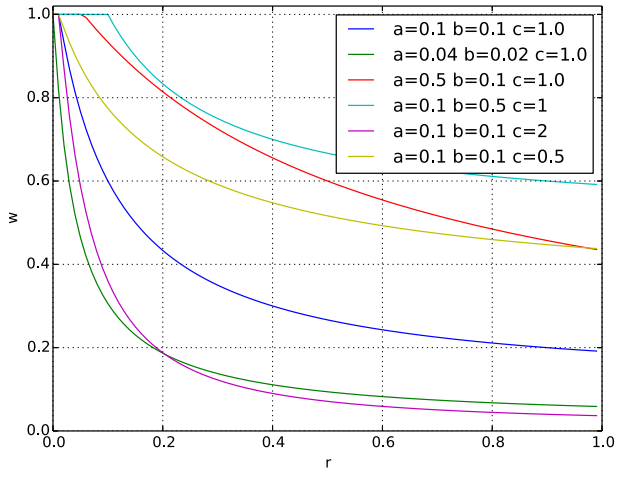

Fig. 2. Overview graph to illustrate the behaviour of Eq. (9) for a few combinations of the terms a, b and c.

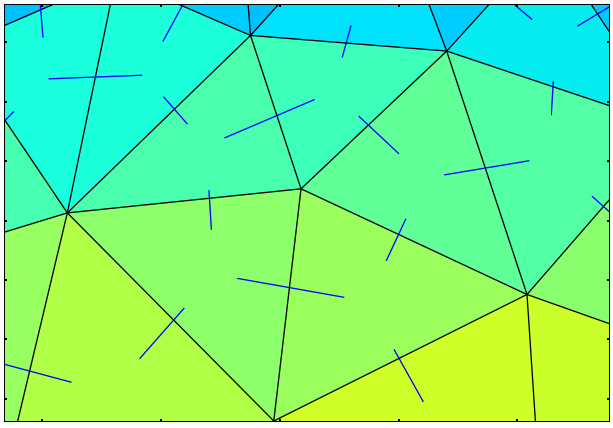

Fig. 3. A schematic zoomed view of the constraint weights between model cells.

can be done on a coarser mesh which speeds up the procedure significantly.

2.2. Synthetic refraction seismic modeling

The forward problem is to simulate the ray propagation for a given slowness distribution $s(\mathbf{r})$ to predict the *first arrival* times using Dijkstra's algorithm (Dijkstra, 1959). The total travel time is the integral over the ray path l

$$t = \int_l dt = \int_l \frac{dl}{v} = \int_l s dl \tag{3}$$

The modeling domain is subdivided into M model cells, where each cell has a constant slowness, s_j. In this discrete form the integral can be expressed as the sum

$$\boldsymbol{t} = \sum_{j=1}^{M} l_j s_j \tag{4}$$

where l_j is a path segment of l. This equation can also be concisely formulated as a matrix-vector product describing the travel times for all ray paths

$$\mathbf{t} = \boldsymbol{L}\mathbf{s} \tag{5}$$

where $\mathbf{t}$ is the travel time vector for the N measured ray paths and $\mathbf{s}$ is the slowness vector containing the slowness values s_j. The $N \times M$ matrix $\boldsymbol{L}$ is the so-called path matrix. The elements L_{ij} are the path lengths of the ith ray through the jth element. Each ray only covers a few cells, making this matrix sparse. The travel time estimation method used here is the path method by Moser (1991). The ray paths are restricted to the edges of the mesh and since only the paths created by the mesh can be used, the travel times will be overestimated. The overestimation can be reduced by increasing the mesh refinement. Dijkstra's algorithm is chosen as it enables the problem to be solved in accordance with Huygens principle and it can be rapidly implemented and solved on standard computers. Dijkstra's algorithm finds the shortest paths from the mesh node where the source of the P-wave is located to the other nodes at the surface, through the mesh, thus constructing the $\boldsymbol{L}$-matrix.

2.3. Inversion

The inversion scheme is based on several meshes. A coarse and resolution-dependent parameter mesh represents the cells where resistivities and velocities are determined. Forward calculations are carried out on a refined mesh using the secondary potential approach. For flat topography, primary potentials are calculated analytically on the forward mesh. In case of topography they are obtained by an additional simulation using a highly refined primary mesh and interpolation on the forward mesh. The employed inversion method uses the Gauss-Newton method with inexact line search by using the methodology of Günther et al. (2006).

Geophysical point data d_i, i.e., apparent resistivities for ERT and travel times for seismic refraction, are stored in a data vector $\mathbf{d} = (d_1, \ldots, d_D)$ with the length D. The parameter distribution, i.e., resistivity and velocity, is represented by a number of M model parameters m_j yielding the model vector $\mathbf{m} = (m_1, \ldots, m_M)$ holding the logarithmic values to ensure positivity. The forward response vector of a model $\mathbf{m}$ is described as $\mathbf{f(m)}$. The task of minimizing the difference between the data and model response is performed with respect to the L_2-Norm, yielding the least-squares method. In order to account for the data errors ϵ_i, an error-weighting is used resulting in the minimization of the data objective function

$$\phi_d(\mathbf{m}) = \sum_{i=1}^{D} \left| \frac{d_i - f_i(\mathbf{m})}{\epsilon_i} \right|^2 = \left\| \mathbf{D}\left(\mathbf{d} - \mathbf{f}(\mathbf{m})\right) \right\|_2^2 \tag{6}$$

with $\mathbf{D} = \mathrm{diag}(1/\epsilon_i)$.

The inversion starts with a model $\mathbf{m}^0$, which is usually a homogeneous halfspace for ERT and horizontally layered subsurface with increasing velocities for seismic. Subsequent models $\mathbf{m}^{k+1}$ are obtained by

$$\mathbf{m}^{k+1} = \mathbf{m}^k + \boldsymbol{s}^k \Delta \mathbf{m}^{\mathbf{k}}.$$

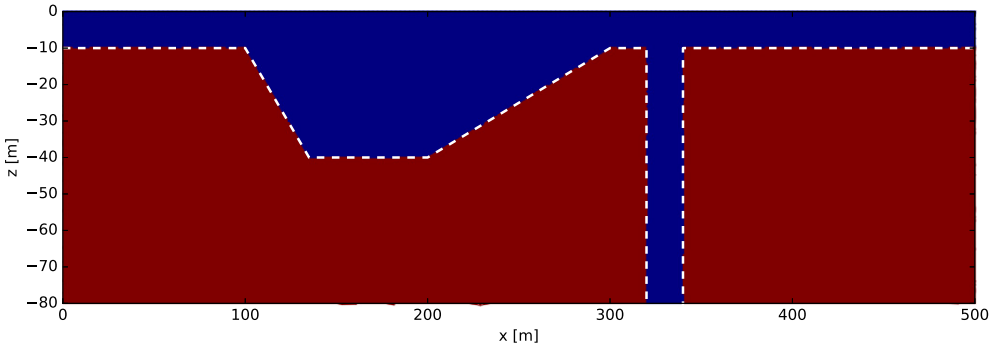

Fig. 4. Model 1: sediment (blue) with $\rho = 100\ \Omega$ m, $v = 1000$ m/s, bedrock (red) with $v = 5000$ m/s, $\rho = 1000\ \Omega$ m.

where $\Delta\mathbf{m}^k$ is the model update and $\boldsymbol{s}^k$ a line search factor. The model has to be regularized in order to produce a unique solution. In order to constrain the model, a functional Φ_m is constructed and weighted by the regularization parameter λ, yielding the objective function

$$\Phi = \Phi_d + \lambda\Phi_m \rightarrow \min \quad \text{with} \quad \Phi_m = \|\boldsymbol{Cm}\|_2^2 .$$

Here, $\boldsymbol{C}$ is a discrete first-order derivative (Günther et al., 2006). Application of the Gauss-Newton method on minimizing Φ leads to

$$\Delta\mathbf{m^k} = \left(\boldsymbol{J^T D^T D J} + \lambda \boldsymbol{C^T C}\right)^{-1} \left(\mathbf{J^T D^T D}\,(\mathbf{d} - \mathbf{f(m)}) - \lambda \boldsymbol{C^T C m}\right). \quad (7)$$

This equation is solved and the model is updated until Φ plateaus. If data errors are well chosen, the regularization parameter controlling the smoothness of the model should be chosen such that the chi-square value $\chi^2 = \Phi_d / N$ equals 1.

The visibility of the inversion results is controlled by the data coverage. This measure shows to which extent model cells are contributing to the data. The Jacobian matrix $\mathbf{J}$ holds the partial derivatives $S_{ij}(\boldsymbol{m}^n) = \frac{\partial f_i(\boldsymbol{m}^n)}{\partial m_j}$. The coverage vector sums up the absolute value of all rows, i.e. of all data for each model cell.

2.4. Structurally coupled inversion

The structurally coupled cooperative inversion (SCCI) approach requires no canonization of a final main earth model, but leads to one model for each method. After some separate inversions

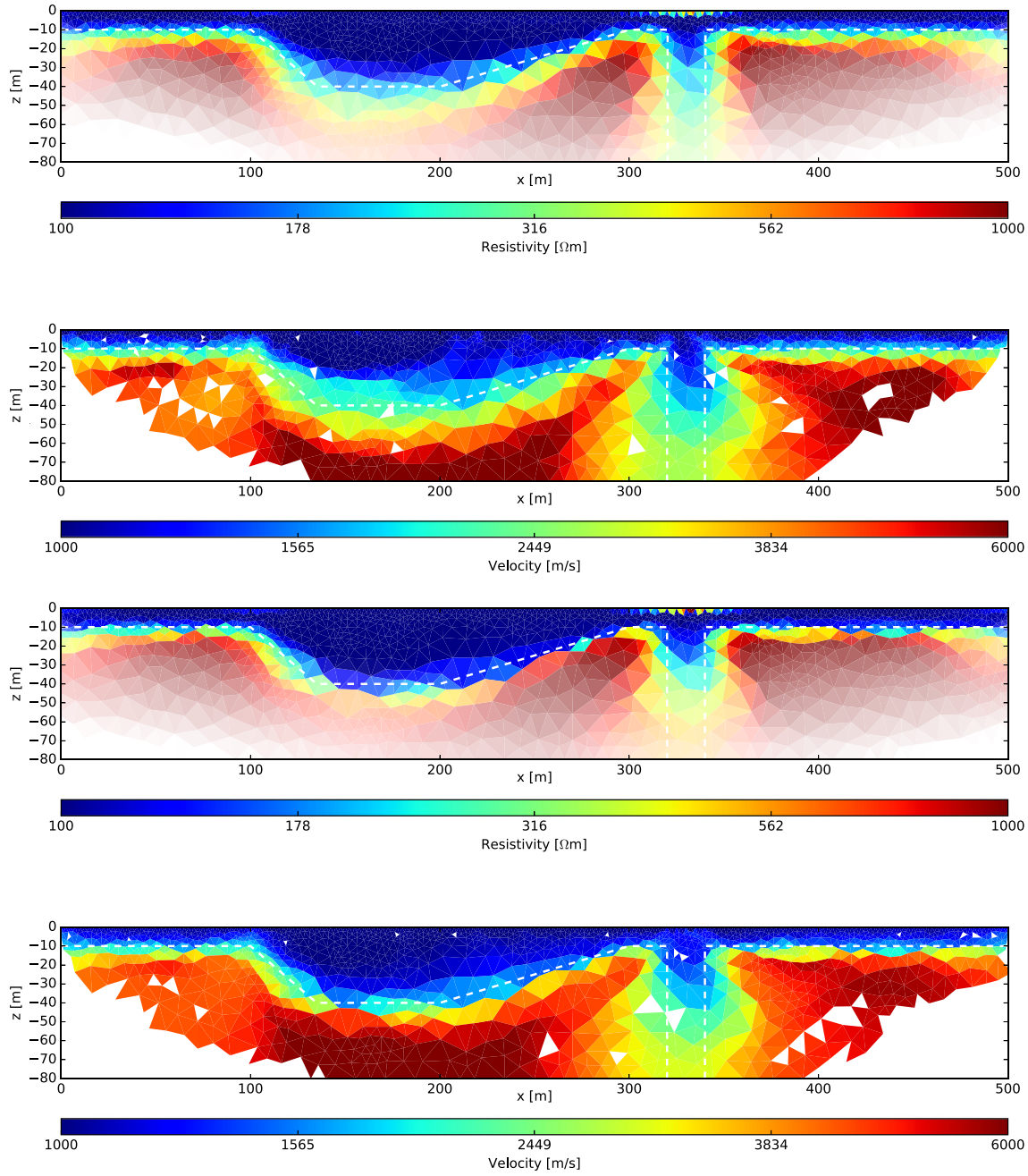

Fig. 5. Model 1 inverted profiles. a) Separate resistivity section and refraction section. b) Structurally coupled resistivity section and refraction section.

are performed, structural information is exchanged through the derivative matrices for each coupled inversion step until convergence for both parts is reached. The overall approach is depicted in Fig. 1.

The roughness operator $\mathbf{C} \in R^{(B)\times M}$ consists of B rows where B is the number of boundaries. Each row is weighted by a diagonal matrix spanned by a vector $\mathbf{w_c}$

$$\mathbf{C} = \mathrm{diag}\,(\mathbf{w^c})\,\mathbf{C_0}. \tag{8}$$

$\mathbf{C_0}$ is the classic (unweighted) smoothness operator. The individual elements w_i^c describe the penalty factors for the individual model boundaries, thus enabling the control of the model characteristics, e.g. regarding the direction of the contrast (Coscia et al., 2011). It also enables the integration of sharp boundaries or may be exploited to iteratively reinforce structures using an iterative L_1-norm mapping (Claerbout and Muir, 1973).

This principle is exploited here to exchange structural informations between the models. Let $\mathbf{r^1} = \mathbf{C}(\mathbf{m^1})$ be the roughness vector of one model m^1. We continue by defining a function with values between 1 (normal penalty) for small gradients and 0 (no penalty) for increasing absolute values of gradients. Günther and Rücker (2006) used an iteratively reweighted least squares (IRLS) function (Claerbout and Muir, 1973). However, we observed that for this method only the main gradients lead to significant reduction of the function and generalize the function of Günther et al. (2010) by introducing another parameter

$$w_i = \left(\frac{a}{|r_i| + a} + b\right)^c \tag{9}$$

Fig. 2 illustrates the three parameters. The value a represents a negligible gradient (of logarithms) and controls the point where the roughness $\boldsymbol{r}$ is large enough to take influence (e.g., 0.1 corresponds to 10% change). The parameter b is used to control the overall value of the constraint weight w_i and moves the curve up and down. The parameter c controls the steepness of the curve, i.e. a large c will result in an overall stronger influence of the coupled model.

The constraint weights can be illustrated by lines between adjacent model cells in Fig. 3 for an example model. Changes occurs predominately in the vertical direction. Cells that are more strongly coupled are illustrated by longer lines between these cells.

Instead of defining mutual constraints (Günther and Rücker, 2006), a combined operator $\mathbf{C_{comb}}$ is used. The diagonal matrices for each method are multiplied, resulting in the expression

$$\mathbf{C_{comb}} = \mathrm{diag}\,(\mathbf{w^{c,\rho}})\,\mathrm{diag}(\mathbf{w^{c,v}})\mathbf{C_0}\ . \tag{10}$$

$\mathbf{C_{comb}}$ is used as a constraint matrix for both inversion methods. This enables the coupling of an arbitrary number of structural models, explicitly being the equation where mutual coupling occurs.

The inversion procedure (Fig. 1) starts with the mesh generation. The electrodes, geophones and shot points are included as nodes in this mesh. Two starting models, ρ_0 (resistivity) and v_0 (velocity) are created. Also different from previous approaches, a couple of separated iterations are performed prior to the coupled inversion in order to generate stable structures in the models before coupling is activated by utilizing the constraint matrix $\mathbf{C_{comb}}$.

2.5. Cluster analysis

The basic idea behind clustering is to group data that share similarities in the model parameters and conversely to differentiate data that share no similarities. It can be seen as a sort of unsupervised learning. As there are several ways to learn, there are various cluster algorithms, the choice of which depends on the application. There is a general expectation that seismic P-wave velocity and electrical resistivity are related, e.g., through porosity. The Fuzzy C-means (FCM) algorithm has successfully been applied to geophysical data by Paasche et al. (2006). We have considered the k-means algorithm (e.g., Ghosh and Liu, 2009). However, it has a major drawback common for other clustering algorithms in the need

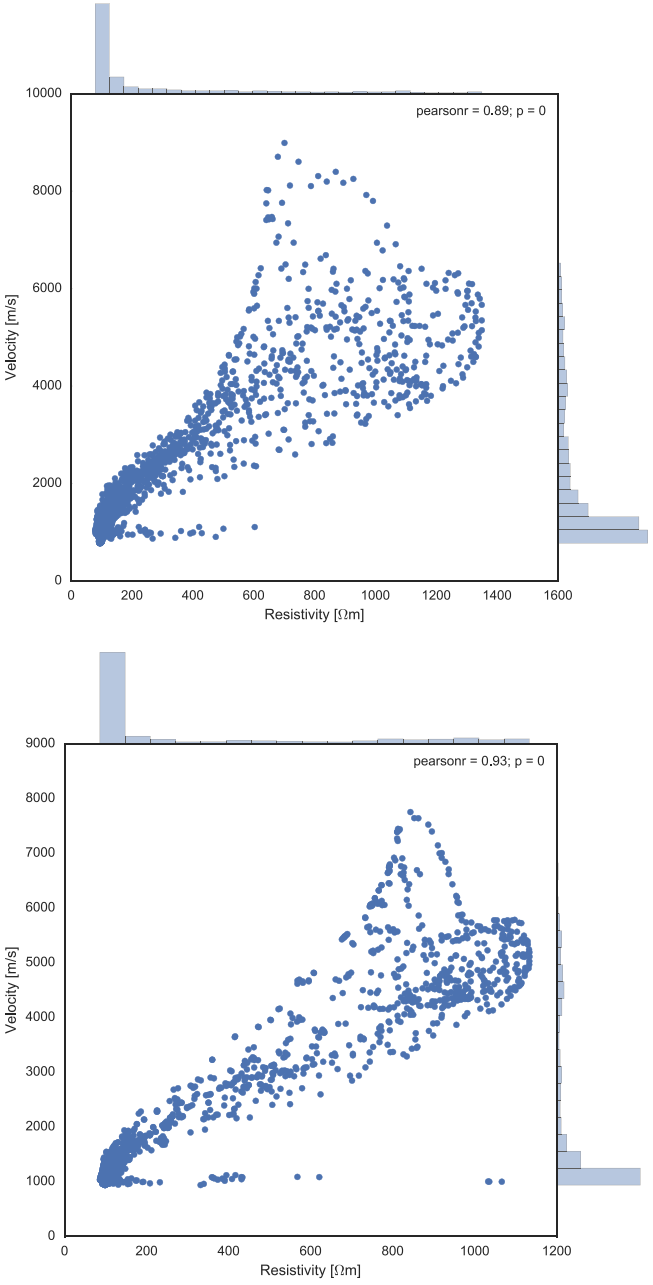

Fig. 6. Model 1 scatter plots. a) Separated model data. b) Structurally coupled model data.

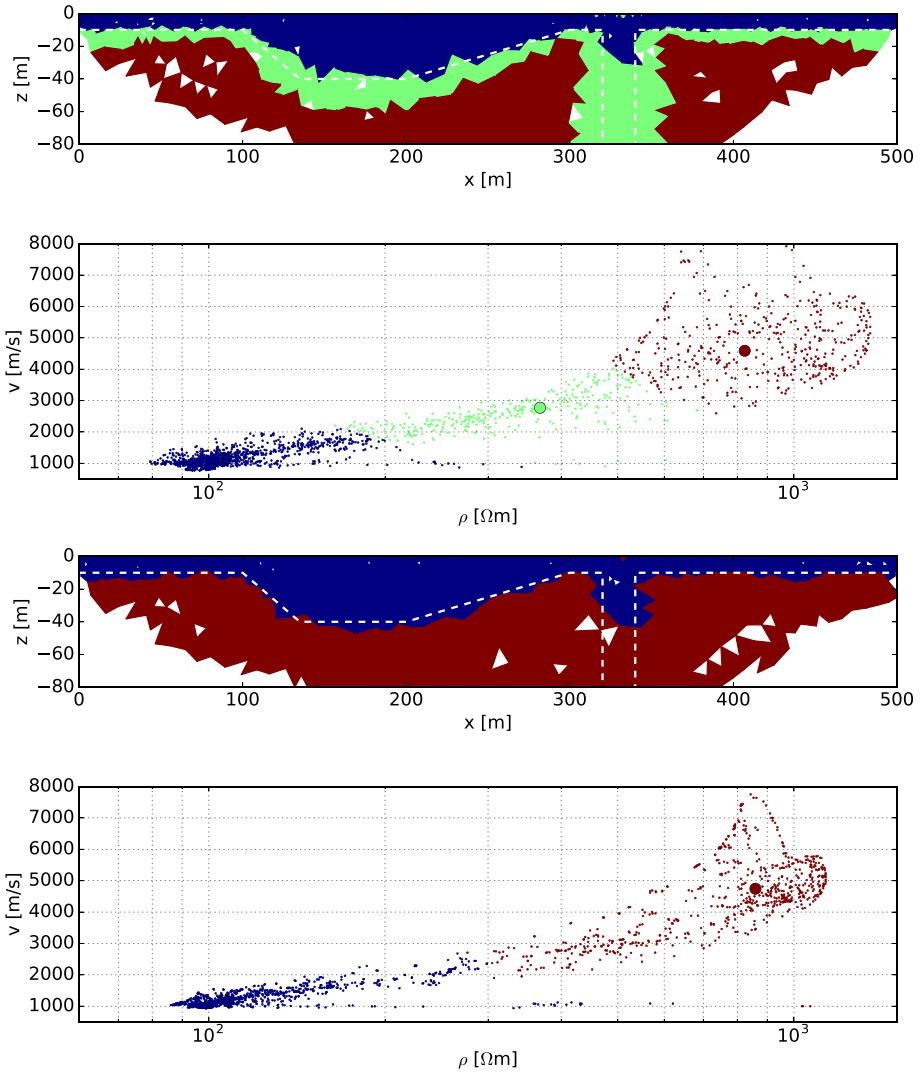

Fig. 7. Model 1 cluster plots of a) separate inversions and b) structurally coupled inversions.

to know the number of clusters, i.e. the number of geological units controlling our data. This requires a-priori information in order to set up the analysis.

After careful consideration of several different algorithms, we have concluded that a variation of the Mean Shift algorithm, rediscovered by Comaniciu et al. (2002) is an appropriate algorithm for our type of data. The algorithm is a data-driven clustering that does not rely on a-priori knowledge. Input is simply given a by means of a feature space with data and a window or bandwidth describing how to view the data. The non-trivial part of the algorithm is of course the bandwidth selection, which is done using the quantile as input. If the quantile is equal to 1/2, the median of all pairwise distances between data is used for bandwidth estimation. The quantile is defined between zero and one. Generally,

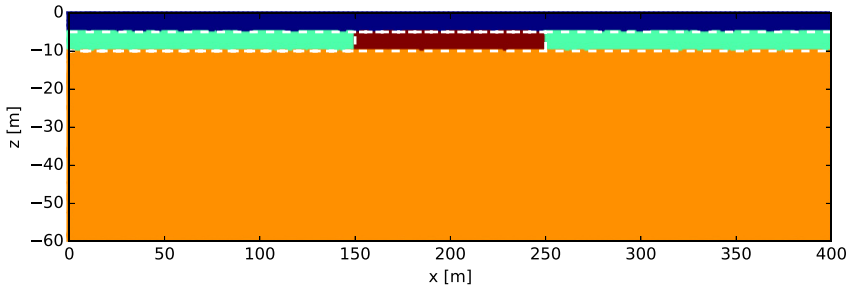

Fig. 8. Schematic view of synthetic model 2.

a small quantile will result in a large number of clusters and a large quantile in limited cluster number. This could be considered a selection of the cluster size, as this is rather an indicative number related to the data itself. Most important, as the clustering algorithm is utilized for comparing coupled and uncoupled inversions, only the data is changed for this comparison, the bandwidth remains identical.

3. Application

The purpose of the following two synthetic models is to verify the performance of the methodology towards field conditions. The purpose of the field example is to show that the methodology also works with actual field data.

3.1. Synthetic model 1

3.1.1. Description

Model 1 (Fig. 4) is 500 m long and consists of 2 units with seismic velocities and resistivities that both increase with depth. The bottom model layer represents bedrock with a resistivity of 1000 Ω m and a P-wave velocity of 5000 m/s. The upper layer represents a clay layer with a resistivity of 100 Ω m and a P-wave velocity of 1000 m/s. The layer interface resembles a valley and dyke profile.

The resistivity model is created by simulating a 101 electrode layout with 5 m spacing using a multiple-gradient array (Dahlin and Zhou, 2004). The 1019 data points were contaminated with Gaussian errors of 3% standard deviation. For the refraction seismic model, the geophones are situated at the electrode positions, with every fourth geophone being used as a shot point. The 1360 data points were subject to Gaussian noise of 1 ms standard deviation.

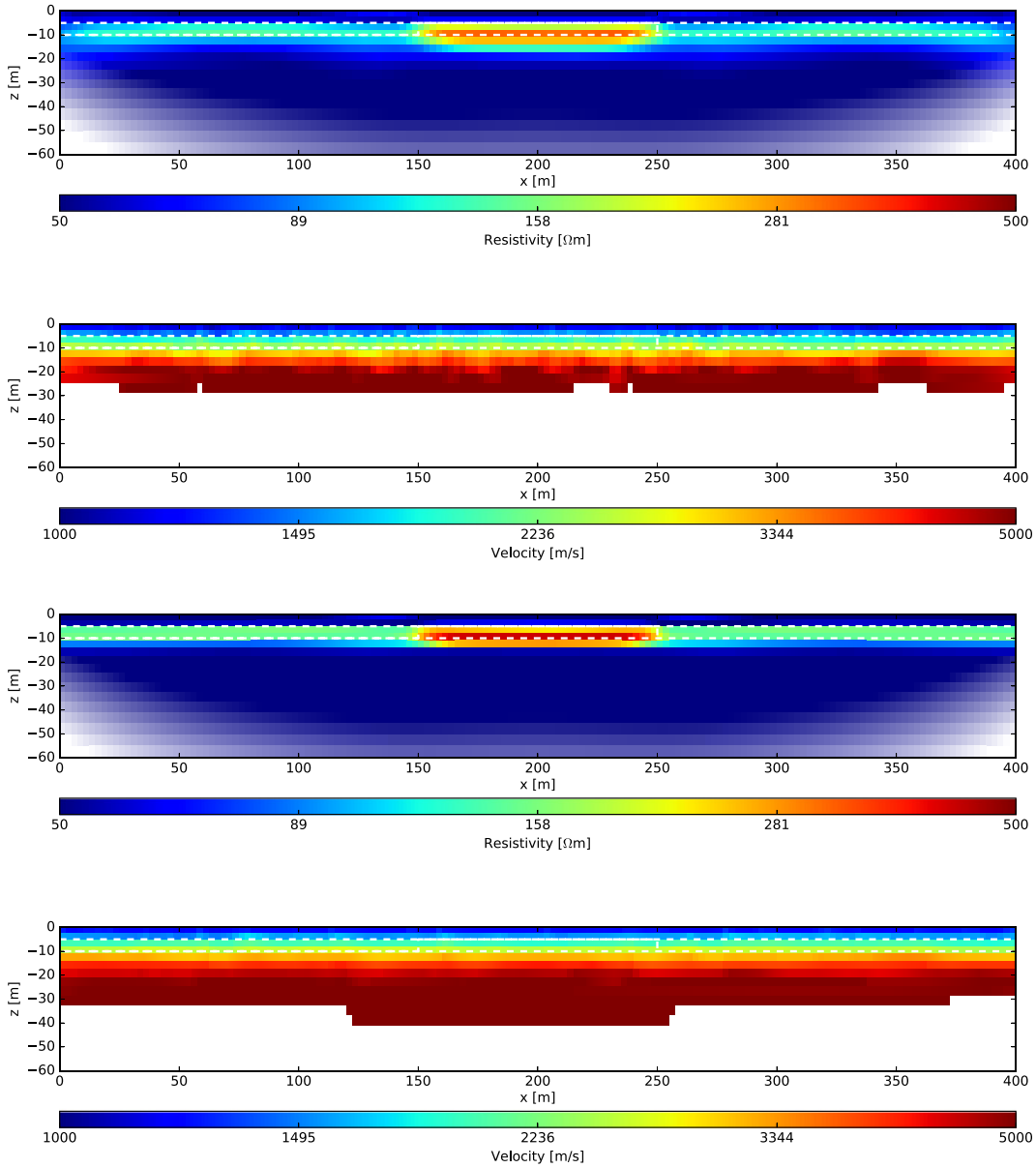

Fig. 9. Inverted sections for model 2. a) Separate resistivity inversion and refraction inversion. b) Structurally coupled resistivity inversion and refraction inversion.

3.1.2. Inversion and statistical comparison

The results from the separate inversion are presented in Fig. 5. The two layers are very well defined in the resistivity section, although the depth penetration fades out quite fast due to the low resistivity on top. The refraction tomography delineates the bedrock layer but produces a somewhat undulating top layer where boundaries are unclear. Both methods show a quite thick transition zone as a result of the smoothness constraints. The inverted values are in the right range, with some overestimation of the velocity. An interpretation would possibly overestimate the bedrock depth. The dyke is imaged by both methods.

The result of the structurally coupled inversion in Fig. 5b shows similar images. However with improved contrasts and thus significantly reduced transition zones, which makes a visual interpretation of the bedrock depth easier. In contrast to the bedrock there is no improvement of the relatively small dyke.

3.1.3. Cluster analysis and cluster plot

The structural coupling clearly increases the correlation between the parameters, with less scatter in the cross-plots in Fig. 6b than in Fig. 6a. A slightly higher coefficient of correlation $r=0.93$ can also be noted for the coupled inversion, compared to 0.89 for separate inversion. The results from the Mean Shift cluster analysis are plotted in Fig. 7 for the separate and coupled inversions, respectively. While the separate inversion results demand a number of three clusters due to the large transition zone, the coupled inversion leads to only two clusters that agrees with the synthetic model. The third cluster appearing in Fig. 7a could be problematic for the interpreter. Possibly leading to the conclusion that there is a third and intermediate layer.

3.2. Synthetic model 2

3.2.1. Description

Model 2, seen in Fig. 8 is inspired by actual field cases that are associated with pronounced equivalence of a thin resistive layer. The model could be regarded as a sequence of different sediments resting on metamorphic rock. Under a clayey-silty top layer with a resistivity of 50 Ω m there is a layer of coarse-grained sediments. The latter varies in grain size distribution or in the degree of leaching, leading to resistivity variations between 200 Ω m and 500 Ω m. The bedrock is relatively conductive with a resistivity of 50 Ω m. The sediment layers are assumed to be close to each other from seismic point of view and were given a P-wave velocity of 1200 m/s, whereas the bedrock is quite competent at 5000 m/s. Gaussian errors were added in the same way as for model 1. A rectangular grid was used in order to better resolve the underlying geometry. Model values are specified in Table 1.

3.2.2. Inversion and statistical comparison

In Fig. 9a the results from the separate inversion are shown. The correspondence to the synthetic model (Fig. 8) is clearly noticeable in both the resistivity and refraction section. As for model 1, there is also some smoothing, particularly at the lower boundary.

The structurally coupled sections in Fig. 9b are similar, especially for the interface between the upper layers, as there is no velocity contrasts that could improve resistivity. Smoothing is still visible, but in general the different regions are well separated, particularly the lower boundary.

3.2.3. Cluster analysis and cluster plot

Studying the histograms in Fig. 10 we can observe an improvement in the overall tidiness of the inverted model data after coupled inversion. The correlation between resistivities and velocities are also improved. The cluster plots in Fig. 11 show the improvement that structural coupling can provide. There is improved correlation between the resistivity and the seismic velocity as shown by the reduced scatter in the cluster plot. Especially notable is the improved resolution below the main anomaly for the coupled inversion. The bottom layer shows much less variability, making the interpretation of this layer more straight forward.

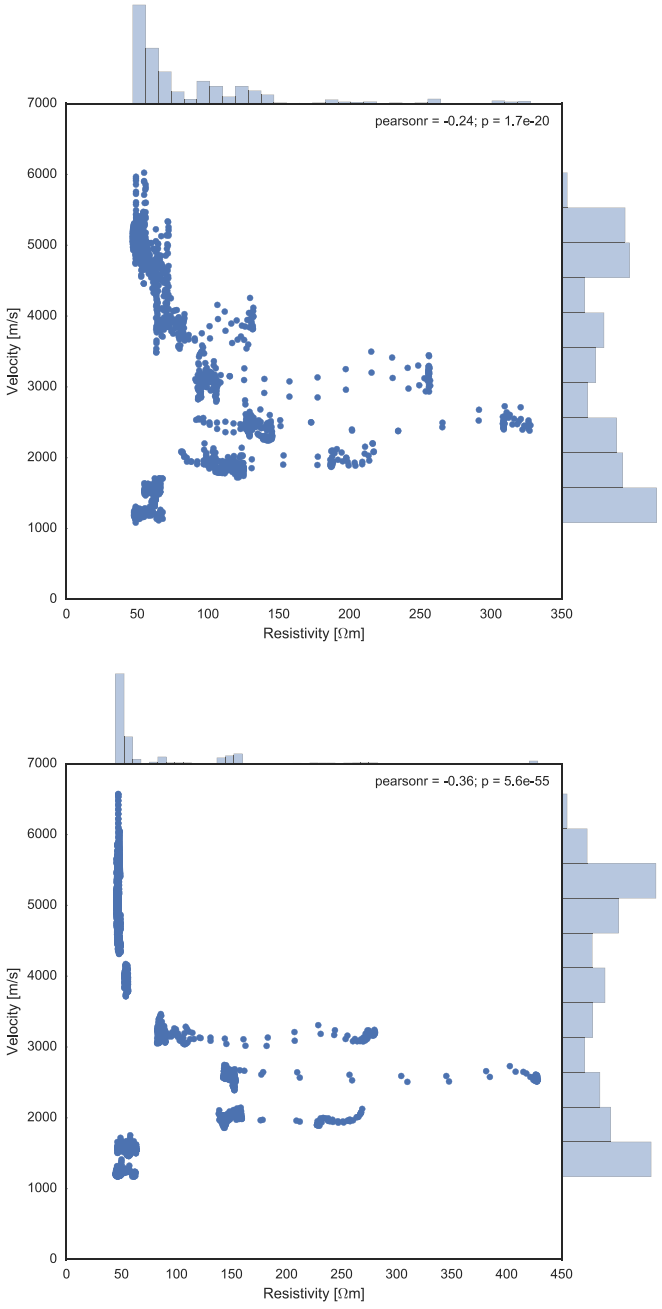

Fig. 10. Model 2 scatter plots. a) Separated model data. b) Structurally coupled model data.

3.3. Field case - Vagnhärad

The field case presented here is from a slope stability investigation in Vagnhärad, Sweden. The geological setting is a depression in the bedrock, the Trosa river valley, filled with mainly glacial clay. Slope failures are caused by erosion in and around the Trosa river, which have reduced the thickness of the clay deposits close to the river and increased the steepness of the valley slopes. In 1997 a large slope failure caused an area of more than 10,000 m^2 to slide into the

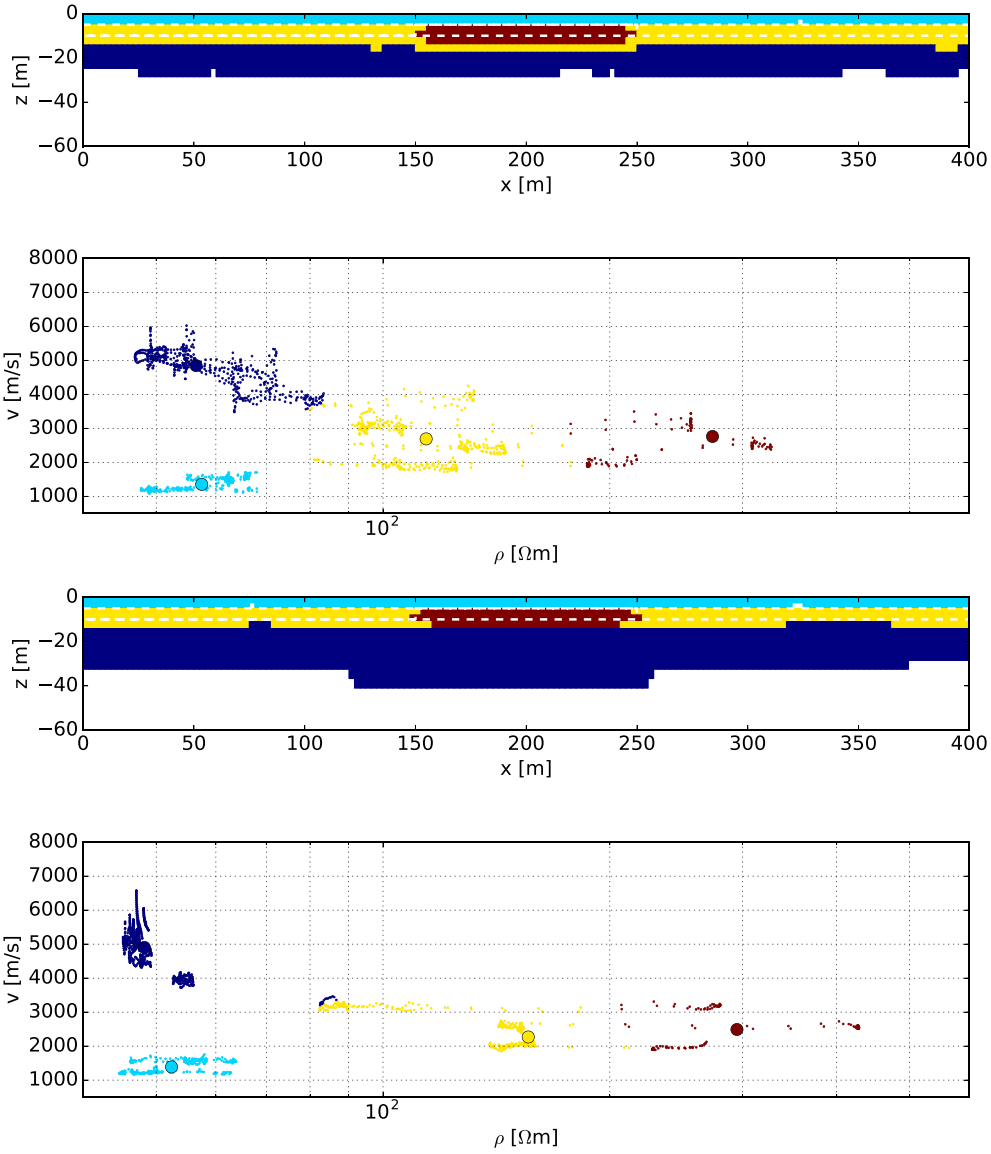

Fig. 11. Model 2 cluster plots of a) separate inversions and b) structurally coupled inversions.

river. This was caused by an increased pore-water pressure in the clay, due to increased water pressure in a layer of sandy and silty till between the clay and the bedrock. ERT and refraction seismic was carried out to map the thickness and extent of the till. The two methods complement each other, with the resistivity having a larger contrast between the clay and the till and the velocity having a larger contrast between the till and the bedrock. The ERT measurements were carried out using a modified version of the ABEM Lund Imaging System, where a Booster SAS2000 acted as current transmitter and the receiver was based on a 24 bit A/D converter. The base electrode separation was 2 m with an 81 electrode spread, giving a total layout of 160 m, using a Wenner-Schlumberger-array, resulting in 934 data points. The refraction seismic survey was carried out with a classic refraction setup using a 24 channel ABEM Terraloc Mk6 and 10 Hz geophones at 2.5–5 m separation. Shot points were placed with a large spacing designed for classic refraction analysis and not full tomography, hence containing a mere 85 data point.

Table 1
Model 2 layer values.

Value type	Resistivity [Ω m]	P-wave vel. [m/s]
Layer 1	50	1200
Layer 2	200	1200
Layer 2 -mid	500	1200
Layer 3	50	5000

3.3.1. Inversion

In both images of Fig. 12 the bedrock layer is well resolved with a clear transition zone between the top and bottom layers. Structural coupling yields a slightly smoother model, apparent in both the resistivity and refraction models.

As for the previous synthetic cases, separate and structurally coupled inversion is carried out and the results are then compared. In order to make the separate and coupled inversions comparable, the vertical and horizontal smoothness constraints is the same for all inversions. The resistivity yields a three layer model. The bottom layer is highly resistive ($\rho \geq 250$ Ω m). The middle layer is conductive with resistivities ranging from 10–250 Ω m. The top layer has a small thickness and is resistive. The refraction result also gives a three layer

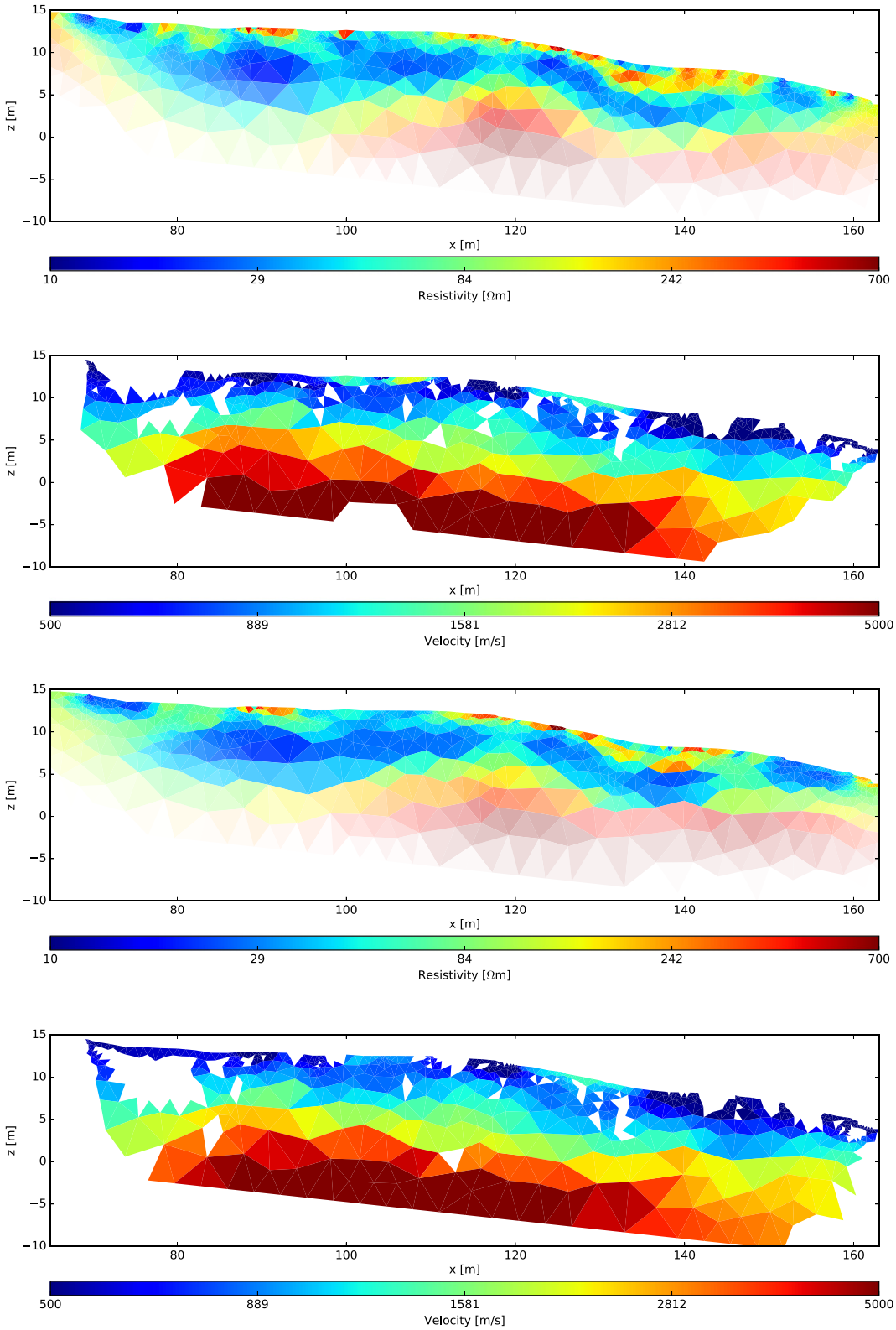

Fig. 12. Field case inversions. a) Separate resistivity and refraction inversion sections. b) Structurally coupled resistivity and refraction inversion sections.

model with the bottom layer having high velocity of 3000–5000 m/s, the mid layer having intermediate velocity of around 1000 m/s and the top layer having low velocity down to 500 m/s. The three layers in the two models are clearly not coincident. It can be seen that the bottom layer has an even surface in the seismic result while it undulates more in the resistivity result. After coupled inversion it can be seen that the two models are more coherent, and that the undulation of the bottom layer has decreased.

3.3.2. Cluster analysis and cluster plot

As there is a weak spatial correlation between the changes in velocity and resistivity in the data, we assume that structural coupling will not enhance or delineate such features. The relevance of this case is dependent on the fact that the inversion should not be driven by constraints but by the data.

The cluster analysis shown in Fig. 13 yield models that are similar, but differ in the respect that the layers are horizontally more regular for the coupled inversion. It becomes apparent that the data density for the inverted sections is very much concentrated to the upper parts of the model. This upper part generally contains low velocities and low resistivities. Correlation between velocity and resistivity data is improved, from 0.53 to 0.63. However, results from the cluster analysis show that scattered pieces of bedrock clusters appear near the surface. The coupled inversion leads to models that are more focused, which can be seen by comparing Fig. 14 (note the upper corners to the right of the figures). A possible drawback with the increased data focus is the decreased Pearson *r* correlation, 0.6 for the coupled inversion compared to 0.7 for the separate.

Fig. 14 shows the corresponding cluster plots. The Mean Shift algorithm determines three clusters for both inversions.

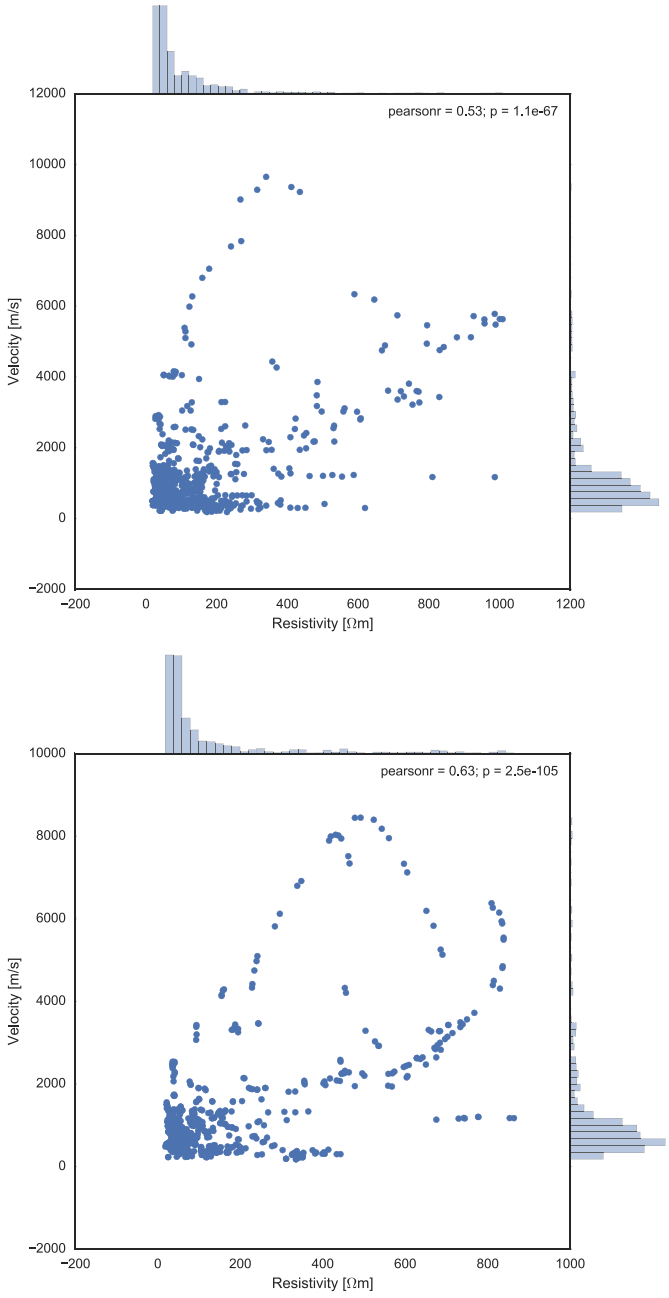

Fig. 13. Field case result scatter plots. a) Separate inversion. b) Structurally coupled inversion.

4. Discussion and conclusions

The results obtained from the synthetic models demonstrate clearly that an exchange of structural information between resistivity and velocity is beneficial for the ability to delineate layers and structures in the subsurface. The equivalence problem is addressed, and alleviated, by the fact that more than one geophysical method is used. The use of structural coupling relies on the assumption that the contrasts in the parameters, however small, are spatially coinciding. Therefore it is necessary to have an understanding for the local geology. The fact that the structural coupling is objective in the sense that it does not enhance structures that are not common is a very important feature.

The utilization of clustering analysis, such as the used Mean Shift cluster algorithm, shows improvements in automating the characterization of geological zones in the models. The benefit from automation and clustering lays both in the improved single geophysical inverted models and in the simplified cluster result that can be delivered to non-experts. An area where further research will be needed is the development or selection of cluster algorithms that are well adapted to the observed data distribution. A toolkit of several algorithms would likely to be the outcome of such research.

The need to integrate in-situ geotechnical methods like CPT, core-drilling and geophysical borehole logging into the inversion modeling is an urgent and natural development for the methodology. This provides further insight into the relationship between the physical parameter and the rock type or degree of weathering.

The conclusions can be summarised as follows:

- Structurally coupled inversion can enhance the resolution of structures and aid in the interpretation of combined geophysical results.
- The coupled inversion method described is data-driven (in opposite to constraint-driven), truly reflecting results that responds to the data.
- The use of clustering algorithms such as mean shift can aid the geophysical interpretation by identifying and enhancing common petrophysical contrasts in areas of interest.
- Adding more information to aid the inversion should be a way forward, and this could for example be results from down-hole methods such as cross-hole GPR, CPT-resistivity and geophysical borehole logging.

Acknowledgements

This work has been financed by The Swedish Research Council Formas, (ref no. 2009-797) as part of the GESP project for Environmental Assessment of Road Geology and Ecology in a System Perspective in cooperation with Dept. of Engineering Geology at Royal Institute of Technology (KTH) in Stockholm. Funding was also provided by BeFo, Swedish Rock Engineering Research Foundation, (ref. 314) and SBUF, The Development Fund of the Swedish Construction Industry, (ref. 12718) as part of the Geoinfra-TRUST framework (http://www.trust-geoinfra.se/). Leibniz Institute for Applied Geophysics (LIAG) and Lund University (LU) provided in-kind support. We also wish to thank Niklas Linde and Roger Wisén for providing highly valuable feedback on the manuscript.

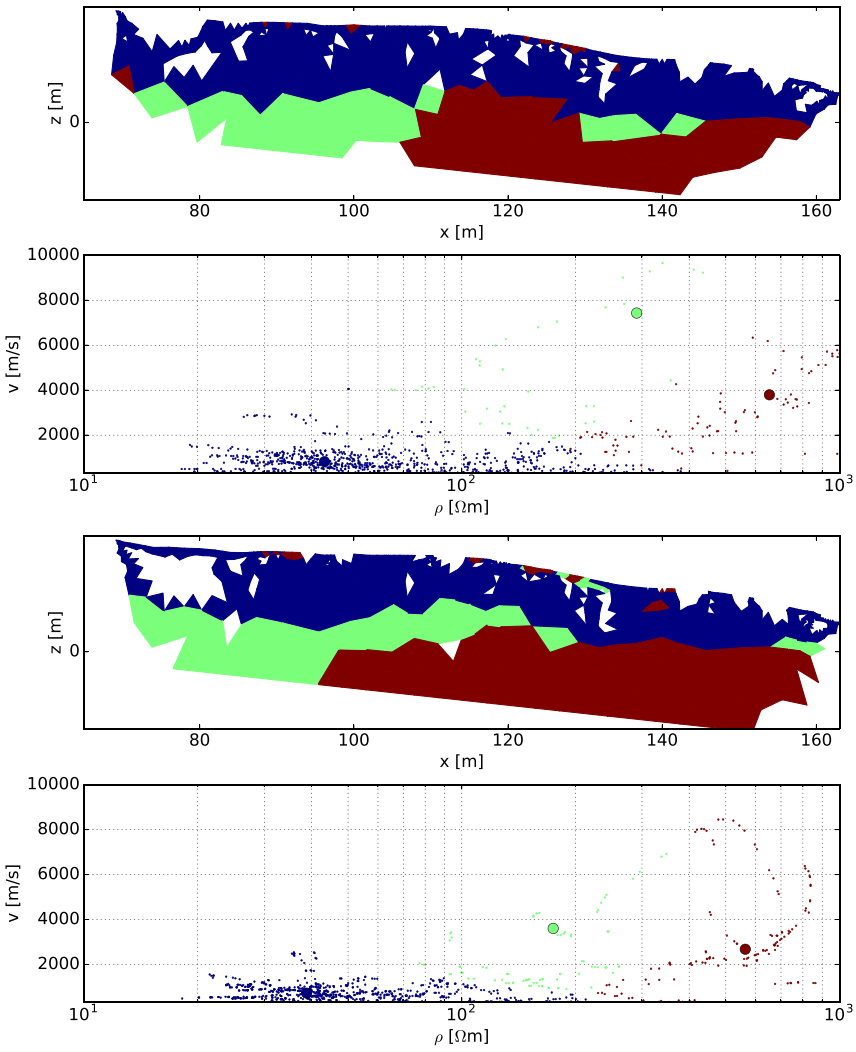

Fig. 14. Cluster plots of the Vagnhärad field case. a) Separate inversion cluster plot. b) Structurally coupled inversion cluster plot.

References

Archie, G.E., 1942. The electrical resistivity log as an aid in determining some reservoir characteristics. I. Pet. Technol. 5, http://dx.doi.org/10.2118/942054-G.

Bedrosian, P., Maercklin, N., Weckmann, U., Bartov, Y., Ryberg, T., Ritter, O., 2007. Lithology-derived structure classification from the joint interpretation of magnetotelluric and seismic models. Geophys. J. Int. 170 (2), 737–748.

Bosch, M., 1999. Lithologic tomography: from plural geophysical data to lithology estimation. J. Geophys. Res. Solid Earth 104 (B1), 749–766. (19782012).

Cavinato, G., Di Luzio, E., Moscatelli, M., Vallone, R., Averardi, M., Valente, A., Papale, S., 2006. The new Col di Tenda tunnel between Italy and France: integrated geological investigations and geophysical prospections for preliminary studies on the Italian side. Eng. Geol. 88 (1), 90–109.

Claerbout, J.F., Muir, F., 1973. Robust modeling with erratic data. Geophysics 38 (5), 826–844.

Comaniciu, D., Meer, P., Member, S., 2002. Mean shift : a robust approach toward feature space analysis. IEEE Trans. Pattern Anal. Mach. Intell. 24 (5), 603–619.

Coscia, I., Greenhalgh, S., Linde, N., Doetsch, J., Marescot, L., Günther, T., Green, A., 2011. 3D crosshole apparent resistivity static inversion and monitoring of a coupled river-aquifer system. Geophysics 76 (2), G49–G59.

Dahlin, T., Bjelm, L., Svensson, C., 1999. Use of electrical imaging in site investigations for a railway tunnel through the Hallandsas Horst, Sweden. Q. J. Eng. Geol. Hydrogeol. 32, 163–172. part 2 192MA Times Cited:8 Cited References Count:12.

Dahlin, T., Zhou, B., 2004. A numerical comparison of 2D resistivity imaging with 10 electrode arrays. Geophys. Prospect. 52 (5), 379–398.

Danielsen, B.E., 2010. The applicability of geoelectrical imaging as a tool for construction in rock. . Lund University., Thesis.

Di, Q., Wang, M., 2010. Determining areas of leakage in the Da Ye Dam using multi-electrode resistivity. Bull. Eng. Geol. Environ. 69 (1), 105–109.

Dijkstra, E.W., 1959. A note on two problems in connexion with graphs. Numer. Math. 1 (1), 269–271.

Doetsch, J., Linde, N., Pessognelli, M., Green, A., Günther, T., 2012. Constraining 3-D electrical resistance tomography with GPR reflection data for improved aquifer characterization. J. Appl. Geophys. 78, 68–76.

Gallardo, L.A., Meju, M.A., 2004. Joint two-dimensional DC resistivity and seismic travel time inversion with cross-gradients constraints. J. Geophys. Res. 109 (B3), B03311.

Gallardo, L.A., Meju, M.A., 2011. Structure-coupled multiphysics imaging in geophysical sciences. Rev. Geophys. 49 (1). Mar.

Ghosh, J., Liu, A., 2009. K-Means, Chapman and Hall/CRC Data Mining and Knowledge Discovery Series. Chapman and Hall/CRC., pp. 21–35. book section 2.

Günther, T., Dlugosch, R., Holland, R., Yaramanci, U., 2010. Aquifer characterization using coupled inversion of MRS & DC/IP data on a hydrogeophysical test-site. Ext. Abstract, 23. EEGS Annual Meeting (SAGEEP), April 11–14, 2010; Keystone, CO. vol. 23. pp. 302–307.

Günther, T., Rücker, C., 2006. A new joint inversion approach applied to the combined tomography of dc resistivity and seismic refraction data. 19. EEGS Annual Meeting (SAGEEP), Seattle, USA. pp. 433–438.

Günther, T., Rücker, C., Spitzer, K., 2006. Three-dimensional modelling and inversion of DC resistivity data incorporating topography - II. Inversion. Geophys. J. Int. 166 (2), 506–517.

Haber, E., Oldenburg, D., 1997. Joint inversion: a structural approach. Inverse Prob. 13 (1), 63.

Kemna, A., 2000. Tomographic Inversion of Complex Resistivity. Ruhr-Universität Bochum. Ph.D. thesis.

Lelivre, P.G., Farquharson, C.G., Hurich, C.A., 2012. Joint inversion of seismic traveltimes and gravity data on unstructured grids with application to mineral exploration. Geophysics 77 (1), K1–K15.

Linder, S., Paasche, H., Tronicke, J., Niederleithinger, E., Vienken, T., 2010. Zonal cooperative inversion of crosshole P-wave, S-wave, and georadar traveltime data sets. J. Appl. Geophys. 72 (4), 254–262.

Lines, L.R., Schultz, A.K., Treitel, S., 1988. Cooperative inversion of geophysical data. Geophysics 53 (1), 8–20.

Meju, M., Gallardo, L., Mohamed, A., 2003. Evidence for correlation of electrical resistivity and seismic velocity in heterogeneous nearsurface materials. Geophys. Res. Lett. 30 (7).

Moser, T., 1991. Shortest path calculation of seismic rays. Geophysics 56 (1), 59–67.

Paasche, H., Tronicke, J., 2007. Cooperative inversion of 2D geophysical data sets: a zonal approach based on fuzzy c-means cluster analysis. Geophysics 72 (3), A35–A39.

Paasche, H., Tronicke, J., Holliger, K., Green, A.G., Maurer, H., 2006. Integration of diverse physical-property models: subsurface zonation and petrophysical parameter estimation based on fuzzy c-means cluster analyses. Geophysics 71 (3), H33–H44.

Rücker, C., Günther, T., 2010-2016. Geophysical Modelling and Inversion Library GIMLi - a C++/Python Library for Geophysical Data Analysis. http://www.pygimli.org.

Rücker, C., Günther, T., Spitzer, K., 2006. Three-dimensional modelling and inversion of DC resistivity data incorporating topography. I. Model. Geophysica. J. Int. 166 (2), 495–505.

Tronicke, J., Holliger, K., Barrash, W., Knoll, M.D., 2004. Multivariate analysis of cross–hole georadar velocity and attenuation tomograms for aquifer zonation. Water Resour. Res. 40 (1).

Vozoff, K., Jupp, D., 1975. Joint inversion of geophysical data. Geophysical Journal of the Royal Astronomical Society 42 (3), 977–991.

Wisén, R., Christiansen, A.V., 2005. Laterally and mutually constrained inversion of surface wave seismic data and resistivity data. J. Environ. Eng. Geophys. 10 (3), 251–262.

Wyllie, M.R.J., Gregory, A.R., Gardner, L.W., 1956. Elastic wave velocities in heterogeneous and porous media. Geophysics 21 (1), 41–70.

Zhang, J., Morgan, F.D., 1996. Joint seismic and electrical tomography. Proc. EEGS Symposium on Applications of Geophysics to Engineering and Environmental Problems in Keystone, Colorado. pp. 391–396.